Wavelength-dependent Process Stability in Laser Micro Welding of Copper with High Thickness Ratios

Leonard Plutz*[1,2,3], Dominic Bartels[1,2,4], Claudio Hölbling[3], Christoph Jaskowiak[3], Christian Goth[3], and Michael Schmidt[1,2]

[1]*Institute of Photonic Technologies (LPT), Friedrich-Alexander-University Erlangen-Nürnberg (FAU), Konrad-Zuse-Straße 3-5, 91052 Erlangen, Germany*
[2]*Friedrich-Alexander-University Erlangen-Nürnberg (FAU), Erlangen Graduate School in Advanced Optical Technologies (SAOT), Konrad-Zuse-Straße 3-5, 91052 Erlangen, Germany*
[3]*Vitesco Technologies GmbH, Sieboldstraße 19, 90411 Nürnberg, Germany*
[4]*Bayerisches Laserzentrum GmbH, Konrad-Zuse-Straße 2-6, 91052 Erlangen, Germany*
**Corresponding author's e-mail:* leonard.plutz@lpt.uni-erlangen.de

The increasing electrification of automotive powertrains demands reliable joining technologies for inverter production, particularly for contacting copper busbars to thin copper foils with high thickness ratios. This study investigates infrared (λ = 1030 nm) and green (λ = 515 nm) disk laser radiation for lap joint welding of a 0.6 mm copper busbar onto a 100 µm copper foil (thickness ratio 6:1). Bead on plate welds based on a Design of Experiments identified viable process windows, followed by systematic parameter derivation using the normalized enthalpy β framework across three spot sizes (365 µm, 410 µm, 460 µm) and three welding speeds (100 mm/s, 200 mm/s, 300 mm/s). The HCW/DPW transition was identified at β = 2.34 for green and β = 3.0 for infrared radiation, with IR exhibiting an abrupt penetration depth increase at the transition point. Green laser radiation demonstrated consistently lower standard deviations, with IR radiation exhibiting up to 4.3 times higher scatter. For infrared radiation, stable welding was only achievable under specific conditions, with 300 mm/s being inaccessible for larger spot sizes due to the available laser power range. Green laser radiation offers a significantly wider and more robust process window, making it the preferred source for copper busbar-to-foil contacting in automotive power electronics.
DOI:10.2961/jlmn.2026.02.2012
Keywords: laser micro welding, copper, 515 nm, 1030 nm, disk laser, process stability, LPM2026

1. Introduction

The increasing electrification of automotive powertrains requires the continuous development of reliable and high-precision joining technologies, particularly in inverter and power module production [1]. The ongoing trend in inverter production is toward the development of very compact power electronics converters with high power density [2]. Since the joining process is performed in close proximity to temperature-critical components, minimum heat input is essential [3]. This necessitates the systematic investigation of joining processes for connecting elements with highly pronounced thickness ratios and for joining solid copper busbars to thin copper foils [4]. However, the wavelength-dependent process stability for this specific joining configuration with high thickness ratios has not been systematically characterized.

1.1 Wavelength-dependent Absorption and Process Stability

Copper is one of the most demanding materials for laser-based joining due to its high thermal conductivity, approximately ten times higher than commonly used steels, combined with a room-temperature Fresnel absorptivity below 5 % for infrared radiation at 1030 nm [5]. Although absorptivity increases with temperature to approximately 15 % at melting point [6], this transition is difficult to control, making heat conduction welding with IR sources poorly reproducible. Once a keyhole forms, the multiple reflections within the vapor capillary drastically increase the effective absorptivity, leading to unstable energy coupling and making deep penetration welding prone to spatter and melt ejections [7].

In contrast, lasers operating in the visible spectral range offer substantially improved absorption characteristics for copper. Radiation at a wavelength of 515 nm exhibits a ten times higher initial absorption rate on copper at ambient conditions compared to IR sources at 1030 nm [8]. Upon transition to a molten state, the absorptivity of green laser radiation decreases to approximately 35 % under heat conduction welding conditions [6], while the inverse holds for IR radiation at 1030 nm [9] (see Fig. 1). This wavelength-dependent sign change in the temperature dependence of absorptivity produces a damping effect on the process dynamics at green wavelengths, effectively suppressing the uncontrolled energy coupling that drives spatter formation at the onset of keyhole formation with IR radiation [9].

The practical consequence for process design is significant. Since green laser radiation is absorbed more efficiently in the melt before reaching keyhole depth, less energy is available to sustain the vapor capillary through multiple reflections, thereby limiting penetration depth and inherently shifting the process mechanism toward heat conduction welding. This results in substantially improved weld quality and spatter-free processing. Through heat conduction welding and the absence of a vapor channel, reproducible and controlled welds with a calm melt pool can be achieved with green laser radiation. [10]

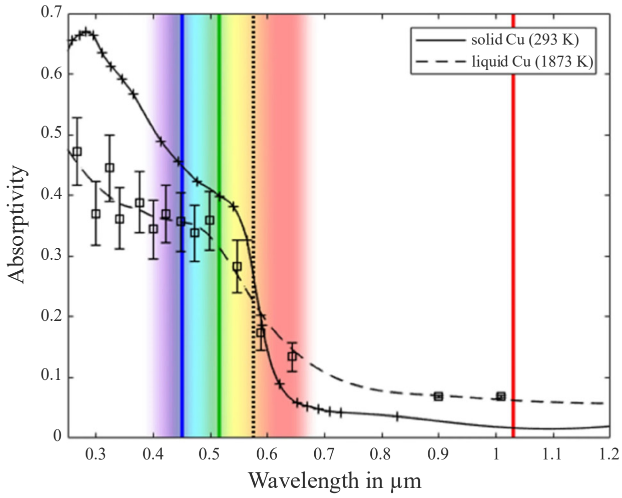

Fig. 1 Wavelength-dependent absorptivity of solid (solid line) and liquid (dashed line) copper measured at room temperature and 1873 K. Figure adapted from [9].

1.2 Laser Joining with High Thickness Ratios

The specific configuration of a thick upper joining partner welded onto a thin lower foil imposes additional constraints on the laser process that go beyond the general challenges of copper welding. The primary technical challenge in laser welding joints with high thickness ratios, such as the connection of busbars to thin foils, is the presence of air gaps between the joining partners [11]. Even minimal gaps between the joining partners significantly disrupt thermal coupling and promote process instabilities, particularly during the transition of the melt from the thin foil into the thicker component. This effect has been reported for foil stack welding in battery applications, where gap-induced variations in heat conduction represent a critical source of process variability [11], [12], [13]. To mitigate these issues and counteract the exponential thermal distortion characteristic of thin materials, the implementation of specialized clamping technology is mandatory to ensure a zero-gap configuration [12], [13].

Furthermore, experimental and numerical investigations in foil stacks for battery applications have shown that the air volume entrapped within the stack is the root cause for the formation of weld undercuts at both the top and bottom surfaces of the seam. As the laser melts the foils, the volume previously occupied by air gaps is eliminated, leading to a localized volume reduction and a subsequent collapse of the melt pool. This characteristic seam geometry not only influences the cross-sectional area of the joint but can also act as a structural weak point, potentially affecting the mechanical and electrical performance of the battery interconnects. [13]

1.3 Normalized Enthalpy as Process Scaling Metric

To enable a physically grounded comparison of process parameters across varying laser wavelengths, spot sizes and welding speeds, the concept of normalized enthalpy by Hann *et al.* [14] is introduced as a dimensionless scaling metric. The normalized enthalpy β relates the applied laser energy input to the thermophysical properties of the material and is defined according to Ye *et al.* [15] and Döring *et al.* [16] as given in equation (1):

$$\beta = \frac{A \cdot P_L}{h_S \cdot \pi \cdot \sqrt{a \cdot v_S \cdot w^3}} \qquad (1)$$

with the enthalpy at melting temperature $h_s = \rho \cdot c_p \cdot T_m$, where A denotes the absorptivity, P_L the laser power, ρ the material density, c_p the specific heat capacity, T_m the melting temperature, a the thermal diffusivity, v_S the welding speed, and w the beam radius.

1.4 Implications for the Present Study

The reviewed literature demonstrates that green laser sources offer fundamental advantages over IR sources for copper welding in terms of absorption stability, process reproducibility, and reduced spatter formation. However, systematic comparative studies specifically addressing the joining of copper busbars with pronounced thickness ratios onto thin copper foils, as encountered in inverter production, remain scarce. As discussed in sections 1.1 and 1.2, direct wavelength comparisons reported to date have been conducted on bulk material or sheet configurations [6], [8], [9], [17], while studies on thin copper foils are confined to battery applications using green laser radiation exclusively [11], [12], [18]. The inverse configuration relevant to inverter production, a solid busbar welded onto a single thin foil with a pronounced thickness ratio, and the influence of wavelength on the robustness of the stable process window under such geometrically constrained conditions have not been systematically characterized. The present study addresses this gap by conducting a direct comparison of IR and green laser sources under identical joint configurations, geometric boundary conditions and identical spot sizes. The present work advances the state of the art by experimentally determining the HCW/DPW transition enthalpies for both wavelengths under identical joint configurations, by quantifying the shift in the required normalized enthalpy range between bead-on-plate and busbar-to-foil conditions, thereby showing that bead-on-plate process windows cannot be directly transferred to high-thickness-ratio lap joints, and by evaluating process stability quantitatively via the standard deviation of penetration depth across the full spot size/ welding speed matrix for both wavelengths. The following research questions guide the experimental investigation:

1. How do spot size and welding speed influence the resulting weld seam geometry and process stability when parameters are derived from a constant normalized enthalpy condition?

2. How does the laser wavelength, near-infrared (1030 nm) versus visible green (515 nm), affect the stability and reproducibility of the weld depth under otherwise equivalent process conditions, and what differences in required laser power are observed between the two sources?

3. Which combination of wavelength, spot size, and welding speed yields the most stable and reproducible

process window that ensures sufficient penetration into the lower joining partner without risking full penetration of the thin copper foil?

2. Materials and Experimental Setup

This section outlines the materials and specimen preparation, the laser systems employed, and the experimental design and methodology underlying the investigations presented in this work.

2.1 Joining Partners

The joining partners consist of a solid copper busbar with a thickness of 0.6 mm (50 x 15 x 0.6 mm³) and a thin copper foil (Schlenk Metallfolien GmbH & Co. KG, Germany) with a thickness of 100 µm (15 x 6 x 0.1 mm³), resulting in a thickness ratio of approximately 6:1. Both components are made of oxygen-free pure copper (Cu-OF), with surface conditions of as-rolled. The joints are configured in a lap joint arrangement, with the busbar forming the upper and the foil forming the lower joining partner.

For the initial process window investigations, bead on plate welds were performed on solid Cu-OF substrate specimens with dimensions of 50 x 15 x 5 mm³, providing sufficient material thickness to prevent full penetration across the entire parameter range investigated during the DoE. It should be noted that the application of the normalized enthalpy framework in this work is based on simplifying assumptions: the thermophysical material properties are evaluated at room temperature rather than at the actual process temperature, and the absorptivity values reflect effective energy coupling conditions under heat conduction welding rather than the dynamic absorptivity prevailing during deep penetration welding. These assumptions introduce a degree of approximation into the absolute values of β, but are considered sufficient for the purpose of relative parameter scaling and process window identification, consistent with the established application of this framework in the literature. The thermophysical properties of Cu-OF used in this work are summarized in Table 1. Based on the experimentally determined absorptivity values reported by [6] for Cu-ETP, absorptivity values of approximately $A_{1030} = 0.15$ and $A_{515} = 0.35$ are adopted for infrared and green laser radiation respectively, reflecting the effective energy coupling under heat conduction welding conditions. The ratio of these values directly predicts that approximately twice the laser power is required for IR radiation compared to green radiation at equivalent normalized enthalpy conditions. The sensitivity of the results to these assumptions can be assessed directly from Eq. (1). Since β scales linearly with A, an uncertainty in the absorptivity translates proportionally into the absolute β values, but does not affect the relative ordering of parameter sets within one wavelength. A variation of A by ± 20 % would rescale, but not restructure, the process windows and transition thresholds identified in this work, as these were determined empirically on the β scale itself. Regarding the copper grade, Cu-OF and Cu-ETP are both high-purity coppers whose optical properties at the relevant wavelengths are nearly identical, with the surface condition exerting a stronger influence on initial energy coupling than the copper grade. This is confirmed by temperature-dependent absorption measurements performed directly on Cu-OF at a comparable near-infrared wavelength (1064 nm), which show that the initial absorptivity at room temperature is governed primarily by the natural oxide layer thickness rather than by the specific copper grade [19]. The dynamic increase of the effective absorptivity upon keyhole formation is not captured by the constant values adopted here. The β values in the DPW regime therefore represent nominal rather than physical coupling conditions. This predicted power ratio is examined against the experimental results in section 3.1.

Table 1 Thermophysical properties of oxygen-free copper (Cu-OF) used for the calculation of the normalized enthalpy β.

Parameter	Unit	Value
Density ρ	kg/m³	8960
Specific heat capacity c_p	J/(kgK)	385
Melting temperature T_m	K	1356
Thermal diffusivity a	m²/s	1.17×10^{-4}
Absorptivity A_{515}	-	0.35
Absorptivity A_{1030}	-	0.15

All thermophysical properties are evaluated at room temperature [20]. Absorptivity values represent effective energy coupling conditions during heat conduction welding of Cu-ETP, adopted from [6].

2.2 Fixturing and Specimen Preparation

To ensure reproducible joint conditions and minimize the gap between the joining partners, a dedicated clamping fixture was designed and manufactured from aluminum (Fig. 2). The fixture positions the copper foils and the busbar in a defined lap joint configuration and applies uniform clamping force across the entire weld area via spring clamps acting on the upper busbar to minimize the gap between joining partners, approaching a zero-gap condition, which is critical for consistent laser energy coupling and weld depth reproducibility. A copper buffer sheet with a thickness of 0.6 mm (50 x 15 x 0.6 mm) is placed beneath the foil to protect the fixture from laser-induced damage and to provide a defined thermal boundary condition at the lower side of the joint. The fixture further facilitates efficient specimen handling and allows for a high number of parameter combinations to be welded in a single setup without repositioning, while sufficient cooling intervals between consecutive weld seams ensure that prior welds do not thermally influence subsequent ones.

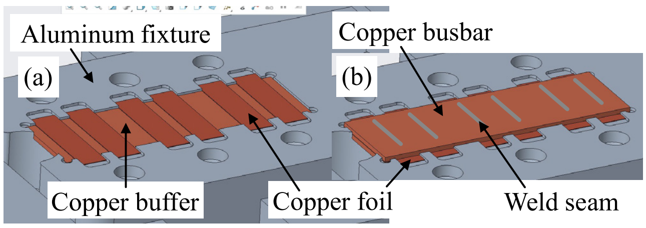

Fig. 2 CAD illustration of the aluminum clamping fixture in disassembled (a) and assembled (b) configuration.

2.3 Laser Systems

Two laser systems operating at different wavelengths are compared in this study. Both systems are manufactured by TRUMPF SE + Co. KG, Germany. The first system is a near-infrared (IR) disk laser of type TruDisk 6001 with a wavelength of 1030 nm and a maximum output power of 6 kW, equipped with a PFO 33-2 scanner optic for beam focusing and weld geometry execution. The second system is a TruDisk 3022 disk laser operating in the visible green spectral range at a wavelength of 515 nm with a maximum output power of 3 kW, using a PFO 33 scanner optic for beam focusing and geometry execution. The key properties of both systems are summarized in Table 2.

Table 2 Properties of the laser beam sources and optical setups used in this work.

Parameter	Unit	Trumpf TruDisk 3022	Trumpf TruDisk 6001
Wavelength λ	nm	515	1030
Max. output power P_{max}	W	3000	6000
Fiber core diameter d_{FOC}	µm	200	200
Progr. Focusing Optics	-	PFO 33	PFO 33-2
Focal length collimation/ optics f_c/ f_F	mm	140/255	150/160
Min. focal diameter d_F	µm	365	339

A schematic illustration of the experimental laser setup is provided in Fig. 3, depicting the optical beam path from the laser source through the scanner optics to the workpiece surface, as well as the positioning of the clamped specimens on the processing stage.

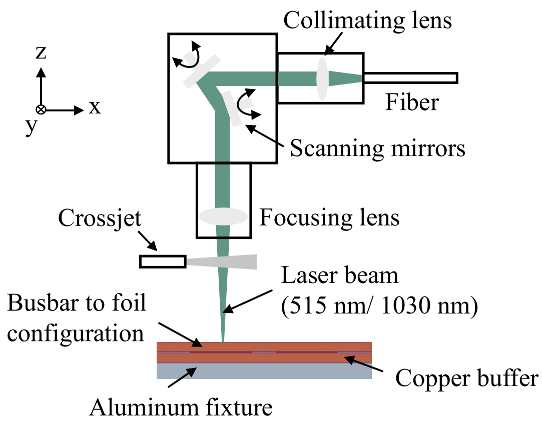

Fig. 3 Schematic illustration of the laser processing setup including the optical beam path and sample positioning.

2.4 Parameter Space and Experimental Design

The experimental investigation follows a two-stage methodology. In the first stage, bead on plate welds were performed on solid Cu-OF substrate specimens (50 x 15 x 5 mm³) based on a structured Design of Experiments (DoE) to identify a viable process window for each laser source independently. The DoE covered a broad range of laser power and welding speed combinations, with the objective of determining the parameter space within which a defined target penetration depth could be achieved. The resulting process windows for the IR and green laser sources served as the calibration basis for the subsequent parameter derivation.

In the second stage, the following parameter combinations for the busbar to foil configuration were derived using the concept of normalized enthalpy β as defined in section 1.3. For each combination of spot size and welding speed, the required laser power was calculated from Equation (1) to maintain a constant normalized enthalpy, ensuring that all parameter sets operate at a physically comparable energy input condition targeting a consistent penetration depth. Three spot sizes (365 µm, 410 µm, 460 µm) were realized by defocusing into the working plane, and three welding speeds (100 mm/s, 200 mm/s, 300 mm/s) were investigated, resulting in a total of nine parameter combinations per laser source. For each combination, the laser power was varied by ± 50 W around the calculated target value to account for process sensitivity near the nominal operating point. For the IR laser source, a welding speed of 300 mm/s could not be realized for the two larger spot sizes (410 µm and 460 µm), as no sufficient bonding between the joining partners could be achieved within the available laser power range.

All experiments were performed n = 3 times per parameter set, producing linear weld seams of 10 mm length, to enable a statistically robust evaluation of process reproducibility. Prior to each weld seam, a stationary laser pulse with a duration of 30 ms was applied at the weld start position for both laser sources. This procedure ensured comparable and reproducible process initiation conditions for both wavelengths, avoiding the transient effects associated with cold material at the start of the weld and enabling a stable keyhole regime to be reached more rapidly at the beginning of the weld seam. For the IR laser source, pulse powers of 2050 W (365 µm) and 2800 W (410 µm, 460 µm) were used. For the green laser source, equivalent pre-pulses were applied at correspondingly adjusted power levels of 1000 W (365 µm) and 1100 W (410 µm, 460 µm), consistent with the absorptivity ratio of the two wavelengths. The welded specimens are characterized by means of metallographic cross-sections prepared perpendicular to the welding direction. To ensure that the steady-state regime of the welding process is captured, the cross-sections are taken at a position of 6 mm from the weld start. The cross-sections are ground, polished and etched with $FeCl_3$-solution. Weld depth and seam width are measured using a light optical microscope of type BX53M (EVIDENT Europe GmbH, Germany). The penetration depth t is measured as the vertical distance from the top surface of the busbar to the deepest point of the fusion zone boundary. With a busbar thickness of 600 µm, t = 600 µm corresponds to the fusion zone just reaching the busbar-foil interface without forming a metallurgical bond, so that reliable joint formation requires $t > 600$ µm. While $t \leq 700$ µm ensures that the 100 µm foil is not fully penetrated. The penetration depth into the foil and the remaining unmelted foil thickness follow directly as t – 600 µm and 700 µm - t.

3. Results and Discussion

The following section presents the experimental results of the bead on plate process window investigations as well as the lap joint welding trials, and discusses the findings with respect to the research questions raised in section 1.3.

3.1 Process Window and Parameter Selection

The results of the bead on plate investigations are presented in Fig. 4 as a function of the normalized enthalpy β for both laser sources. The penetration depth increases with increasing normalized enthalpy for both wavelengths, reflecting the greater energy input per unit volume deposited in the material. However, the two laser sources exhibit distinctly different process characteristics, particularly with respect to the transition between heat conduction welding (HCW) and deep penetration welding (DPW).

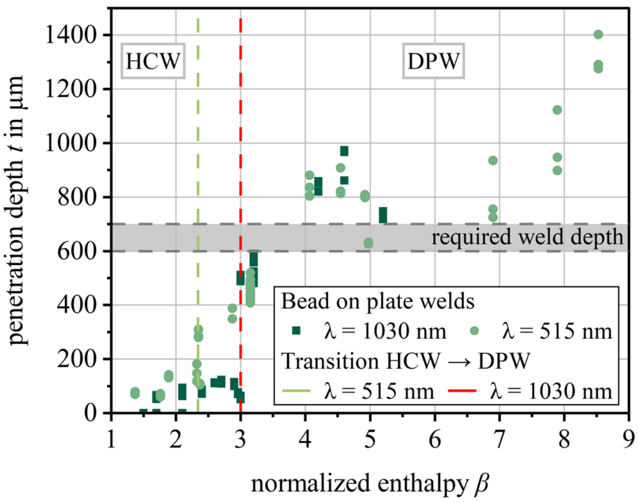

Fig. 4 Penetration depth as a function of normalized enthalpy β using IR and green laser radiation. The vertical dashed lines indicate the transition from HCW to DPW for each wavelength. The shaded region marks the required weld depth range for the busbar-to-foil lap joint application.

For green laser radiation ($\lambda = 515$ nm), the transition from HCW to DPW occurs at a normalized enthalpy of $\beta = 2.34$, whereas infrared laser radiation ($\lambda = 1030$ nm) requires a significantly higher normalized enthalpy of $\beta = 3.0$ to initiate deep penetration welding. Furthermore, the two wavelengths exhibit a different behavior at the transition point with respect to the resulting penetration depth. For green laser radiation, the onset of deep penetration welding is accompanied by a moderate increase in penetration depth from approximately 200 µm to 300 µm, indicating a gradual and controlled transition between the two welding regimes. In contrast, infrared laser radiation exhibits an abrupt jump in penetration depth from approximately 100 µm to 500 µm at the transition point, reflecting the characteristically unstable energy coupling behavior of IR radiation on copper at the onset of keyhole formation. This behavior is consistent with the dynamic absorptivity measurements reported by Kaufmann *et al.* [6], who observed a significantly slower and less defined transition to deep penetration welding for 1030 nm radiation compared to 515 nm radiation. The more gradual transition observed for green laser radiation is understood to result from the higher and more stable initial absorptivity at 515 nm, which enables a progressive increase in energy coupling and melt pool depth without the abrupt threshold behavior characteristic of infrared radiation on copper. As discussed in section 1.1, the wavelength-dependent absorptivity of liquid copper [9] may further contribute to this effect, as the damping behavior at 515 nm inherently limits the energy available for keyhole sustenance.

The target penetration depth range of 600 µm $< t \leq$ 700 µm, required for reliable contacting of the copper busbar to the thin copper foil, is reached in the DPW regime for both wavelengths. For both laser radiation, this depth range corresponds to normalized enthalpy values $3.2 \leq \beta \leq 3.65$. The ratio of the corresponding laser power values required to reach these normalized enthalpy levels is approximately 2:1 (IR:green), consistent with the absorptivity ratio of $A_{1030} = 0.15$ and $A_{515} = 0.35$ adopted in this work. This empirical agreement independently supports the validity of the adopted absorptivity ratio for the relative scaling applied in this work.

3.2 Weld Seam Geometry and Parameter Influence

Following the identification of the target normalized enthalpy range from the bead on plate investigations, the influence of welding speed (100 mm/s, 200 mm/s, 300 mm/s) and spot size (365 µm, 410 µm, 460 µm) on the consistency of the penetration depth is analyzed for the busbar to foil lap joint configuration. It is noted that the normalized enthalpy range required to achieve the target penetration depth of 600 µm $< t \leq$ 700 µm in the lap joint configuration was extended to $2.7 \leq \beta \leq 4.0$, compared to the values identified during the bead on plate investigations. This shift is attributed to the altered thermal boundary conditions inherent to the lap joint geometry, including the presence of the joining interface, the reduced thermal mass of the thin copper foil as the lower joining partner, and the influence of the underlying copper buffer sheet on local heat dissipation. These factors collectively modify the effective energy coupling and heat flow conditions, resulting in a systematic deviation from the process window established on solid substrates.

The results for green laser radiation ($\lambda = 515$ nm) are presented in Fig. 5 as a function of laser power, with the target penetration depth range of 600 µm $< t \leq$ 700 µm indicated by the red dashed reference lines.

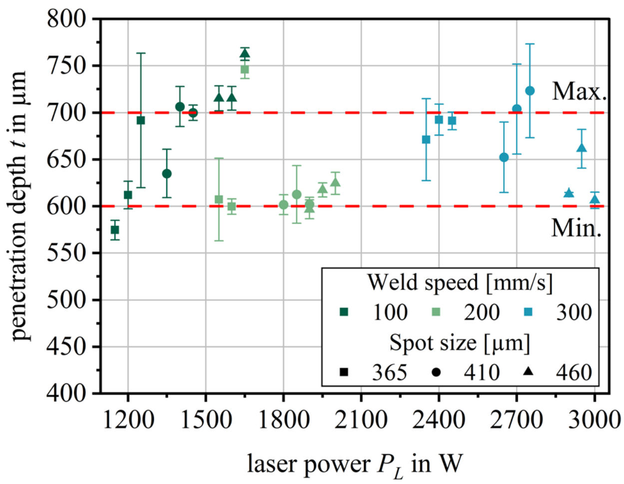

Fig. 5 Process window for green-laser depending on the spot size (symbols) and the welding speed (colors) with normalized enthalpy values between 2.7 and 4.0.

Overall, the majority of parameter combinations yield penetration depths within or in close proximity to the target range, demonstrating the general suitability of the normalized enthalpy framework as a basis for parameter selection. For welding speeds of 100 mm/s and 200 mm/s, most data points fall within the defined process window, with moderate standard deviations indicating a consistent and reproducible welding process. At a welding speed of 300 mm/s, however, a larger deviation in penetration depth is observed, with several parameter combinations exceeding the upper limit of 700 µm or falling below the lower limit of 600 µm. This increased variability at higher welding speeds is attributed not only to the reduced interaction time between the laser beam and the material, but also to the reduced linear energy input per unit length, which narrows the thermal process window for achieving reliable penetration into the thin copper foil without full perforation. In the lap joint configuration with a high thickness ratio, this renders the process more sensitive to minor fluctuations in energy coupling at elevated welding speeds.

With respect to the spot sizes, no systematic trend is observed across the three levels investigated (365 µm, 410 µm, 460 µm), suggesting that the normalized enthalpy framework effectively compensates for the variation in beam geometry through the corresponding adjustment of laser power. The increased standard deviation observed for selected parameter combinations, particularly at higher welding speeds, indicates that process stability is more strongly governed by the welding speed than by the spot size within the parameter range investigated. Fig. 6 presents representative cross-sections of three repeated welds for a stable parameter combination with complete foil bonding (a-c) and a parameter combination exhibiting insufficient penetration into the lower joining partner (e, f), illustrating the consequence of operating below the lower boundary of the stable process window. The dark speckles visible in the etched cross-sections result from the metallographic etching and do not indicate microstructural differences between the parameter combinations. The magnified details (a1) and (a2) resolve the fusion zone at the busbar-foil interface, where a metallurgical bond across the interface is established. Averaged over the three repeated welds of this parameter combination, the fusion width at the interface amounts to 254 ± 30 µm. The heat affected zone adjacent to the fusion boundary is characterized by grain coarsening, as expected for pure copper, which does not undergo solid-state phase transformations.

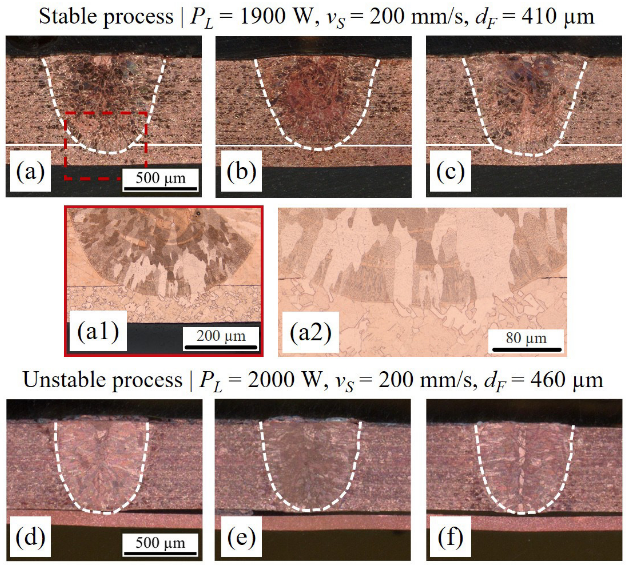

Fig. 6 Cross-sections of three repeated welds for a stable parameter combination (a-c) with magnified details of the busbar-foil interface (a1, a2) and an unstable parameter combination (d-f) with insufficient bonding of the copper foil in (e, f). The white lines indicate the weld seam boundaries. λ = 515 nm.

The results for infrared laser radiation (λ = 1030 nm) are presented in Fig. 7 as a function of laser power. The normalized enthalpy range required to achieve the target penetration depth of 600 µm $< t \leq$ 700 µm in the lap joint configuration extends from $2.9 \leq \beta \leq 4.2$ which is shifted to higher values compared to the green laser source, consistent with the lower absorptivity of copper at 1030 nm and the correspondingly higher laser power required to achieve equivalent energy coupling conditions.

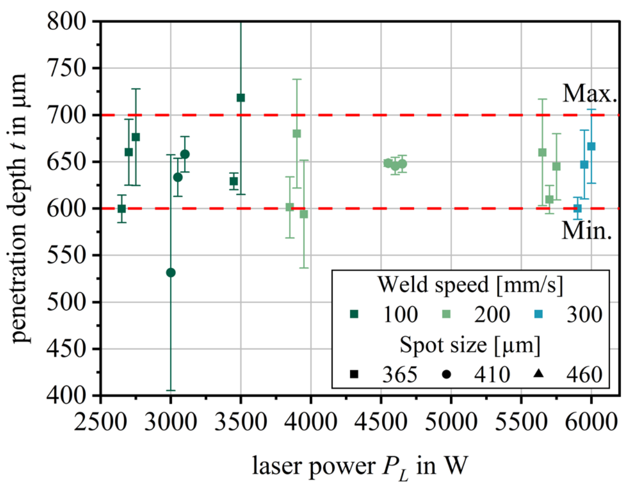

Fig. 7 Process window for IR-laser depending on the spot size (symbols) and the welding speed (colors) with normalized enthalpy values between 2.9 and 4.2.

At the lower boundary of the investigated normalized enthalpy range ($\beta \approx$ 2.9-3.0), significant outliers in penetration depth are observed, with individual measurements deviating considerably from the target range of 600 µm $< t \leq$ 700 µm. This behavior is consistent with the proximity of these parameter combinations to the HCW/DPW transition identified at $\beta = 3$ for infrared radiation, where the process is particularly susceptible to instabilities associated with the abrupt onset of keyhole formation. In this transitional regime, minor fluctuations in energy coupling, inherent to the low and temperature-sensitive absorptivity of copper at 1030 nm, may be attributed to an alternation between heat conduction and deep penetration welding within a single weld seam. This interpretation is consistent with the transition behavior identified in Fig. 4 and with the dynamic absorptivity measurements in [6]. Direct confirmation would require high-speed imaging or multiple cross-sections along the weld seam, which is part of the future work outlined in section 4.

At higher normalized enthalpy values ($\beta > 3.3$), the penetration depth stabilizes and a larger proportion of parameter combinations fall within the target range, suggesting that a more robust deep penetration welding process is established once the keyhole regime is fully developed. Beyond the normalized enthalpy, a general trend toward improved process stability is observed at higher absolute laser power levels ($P_L \geq 4500$ W). Across all spot sizes and welding speeds investigated, parameter combinations requiring elevated laser power consistently yield lower standard deviations in penetration depth. A possible explanation is that a more energetic keyhole is less susceptible to the transient absorptivity fluctuations characteristic of IR radiation on copper, an effect not fully captured by the normalized enthalpy framework alone. This interpretation is consistent with the stability considerations in [9] but cannot be confirmed from the metallographic data alone. It will be examined by the high-speed imaging planned in future work. Nevertheless, the overall scatter in penetration depth remains larger compared to the green laser source across the entire parameter range investigated, reflecting the fundamentally less stable energy coupling behavior of infrared radiation on copper as discussed in section 1.1.

Consistent with both observations, the most stable IR parameter combination is found at a welding speed of 200 mm/s and a spot size of 410 µm at $\beta = 3.3$, where the normalized enthalpy is sufficiently above the HCW/DPW transition threshold and the required laser power is among the highest in the parameter matrix, jointly contributing to the reduced standard deviation observed. Fig. 8 presents representative cross-sections of three repeated welds for a stable parameter combination (a-c) and an unstable parameter combination exhibiting full penetration of the copper foil in (f) (d-f), illustrating the contrast in process reproducibility between the two cases. As for the green laser source, the magnified details (a1) and (a2) resolve the fusion zone at the busbar-foil interface for one representative weld, where a metallurgical bond across the interface is established. Averaged over the three repeated welds of this parameter combination, the fusion width at the interface amounts to 322 ± 43 µm.

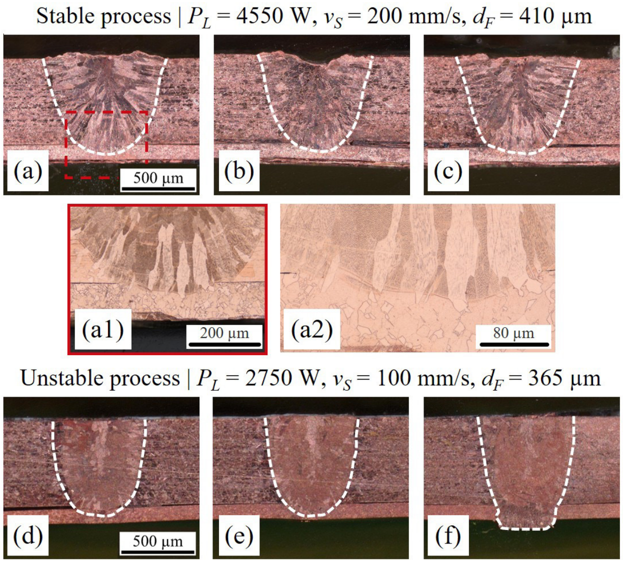

Fig. 8 Cross-sections of three repeated welds for a stable parameter combination (a-c) with magnified details of the busbar-foil interface (a1, a2) and an unstable parameter combination (d-f) with full penetration of the copper foil in (f). The white lines indicate the weld seam boundaries. λ = 1030 nm.

As noted in section 2.4, stable welding at a speed of 300 mm/s could not be achieved for spot size of 410 µm and 460 µm with the IR laser source, reducing the effective parameter matrix. This limitation is specific to the combination of large spot size and high welding speed and reflects a constraint of the available laser system rather than a fundamental instability of the IR process itself. As demonstrated by the stable results obtained at higher normalized enthalpy and power levels, robust IR welding of copper is achievable when sufficient laser power is available.

To quantify the wavelength-dependent difference in process stability, Table 3 summarizes the mean standard deviation of penetration depth grouped by welding speed and spot size. Green laser radiation consistently yields lower standard deviations at welding speeds of 100 mm/s and 200 mm/s, with IR radiation exhibiting 2.0-2.3 times higher scatter. The difference is most pronounced at a spot size of 460 µm, where the IR standard deviation (43.9 µm) exceeds that of green radiation (10.3 µm) by a factor of 4.3. At 300 mm/s, the advantage of green radiation reduces, consistent with the increased process variability observed for both sources at higher welding speeds.

Table 3 Mean standard deviation of penetration depth grouped by welding speed and spot size.

Parameter	SD 515 nm [µm]	SD 1030 nm [µm]	Factor 1030 nm/ 515 nm
100 mm/s	20.5	47.4	2.3x
200 mm/s	15.6	30.8	2.0x
300 mm/s	26.3	29.4	1.1x
365 µm	25.4	37.6	1.5x
410 µm	26.6	31.2	1.2x
460 µm	10.3	43.9	4.3x

Comparing the results for both laser sources, green laser radiation provides a significantly wider and more robust process window for the lap joint configuration investigated, as evidenced by the consistently lower standard deviations summarized in Table 3. While stable processing is achievable with IR radiation under specific conditions, most notably at v_S = 200 mm/s and d_F = 410 µm, this difference is directly attributable to the wavelength-dependent absorptivity of copper, which governs both the energy coupling efficiency and the stability of the keyhole regime as discussed in section 1.1.

4. Conclusion and Outlook

This study investigated the process capability of infrared (λ = 1030 nm) and green (λ = 515 nm) laser radiation for the lap joint welding of a thick copper busbar onto a thin copper foil with a thickness ratio of 6:1, as encountered in inverter and power module production. Parameters were systematically derived using the concept of normalized enthalpy, covering three spot sizes (365 µm, 410 µm, 460 µm) and three welding speeds (100 mm/s, 200 mm/s, 300 mm/s). The following conclusions to answer the research questions of section 1.3 are drawn:

1. Within the normalized enthalpy framework, welding speed is the dominant parameter governing process stability. At 200 mm/s, most parameter combi nations yield penetration depths within the target range with low standard deviations, while 100 mm/s shows a tendency toward over-penetration due to higher linear energy input. At 300 mm/s, significantly increased scatter is observed for both laser sources. The absence of a systematic spot size effect supports the use of the normalized enthalpy framework as a practical process design guideline within the investigated parameter range.

2. Green laser radiation demonstrates consistently lower standard deviations across the entire parameter matrix compared to infrared radiation, reflecting the higher and more stable absorptivity of copper at 515 nm. The HCW/DPW transition occurs at β = 2.34 for green and β = 3.0 for infrared radiation for bead on plate configuration. At the IR transition, an abrupt increase in penetration depth from approx. 100 µm to 500 µm is observed, resulting in significantly increased process variability. Infrared radiation requires approximately twice the laser power of green radiation to achieve equivalent normalized enthalpy conditions, consistent with the absorptivity ratio A_{1030} = 0.15 and A_{515} = 0.35.

3. Green laser radiation at welding speeds of 100 and 200 mm/s provides the most stable and reproducible process window across all spot sizes investigated. For infrared radiation, the combination of v_S = 200 mm/s and d_F = 410 µm at β = 3.3 represents the most favorable operating point, benefiting from both sufficient distance to the HCW/DPW transition threshold and elevated absolute laser power. Overall, green laser radiation offers a significantly wider and more robust process window for the joining of copper components with high thickness ratios, making it the more suitable laser source under the investigated conditions.

The results presented in this study provide a foundation for further investigations into wavelength-dependent laser welding of copper joints with high thickness ratios. Future work will address three aspects. First, the welded joints will be electrically and mechanically characterized through measurements of contact resistance, current-carrying capacity, and joint strength to assess functional performance under realistic operating conditions. Second, high-speed camera recordings of the melt pool will be conducted to correlate the observed process stability differences between the two wavelengths with the underlying melt pool dynamics and keyhole behavior. Third, the investigation will be extended to additional thickness ratios and foil thicknesses to evaluate the transferability of the identified process windows to a broader range of joining configurations relevant to inverter and power module production.

Acknowledgments
The authors gratefully acknowledge funding of the Erlangen Graduate School in Advanced Optical Technologies (SAOT) by the Bavarian State Ministry for Science and Art.

Declaration of AI use
In the preparation of this manuscript, the authors used Claude Sonnet 4.6 (Anthropic PBC, USA) to improve the readability and language of the text. All scientific content, experimental data, results, interpretations, and conclusions are solely the work of the authors. The authors take full responsibility for the integrity and accuracy of the submitted work.

References

[1] A. Ascari and A. Fortunato: Laser dissimilar welding of highly reflective materials for E-Mobility applications, in Joining Processes for Dissimilar and Advanced Materials, Elsevier, (2022), 579.

[2] S. M. I. Rahman, A. Moghassemi, A. Arsalan, L. Timilsina, P. K. Chamarthi, B. Papari, G. Ozkan, and C. S. Edrington: Emerging Trends and Challenges in Thermal Management of Power Electronic Converters: A State of the Art Review, IEEE Access 12, (2024), 50633.

[3] B. N. Reddy, B. Jyothi, G. S. Rao, N. Janaki, P. Swathi, and S. V. R. Reddy: State-of-the-art DC–DC converters for electric mobility and renewable integration: trends, challenges, and future directions, Discov. Appl. Sci. 8, (2026), 160.

[4] Z. Chen and A. Q. Huang: Busbar Design for High-Power SiC Converters, Electronics 13, (2024), 4758.

[5] E. W. Spisz, A. J. Weigand, R. L. Bowman, and J. R. Jack: Solar absorptances and spectral reflectances of 12 metals for temperatures ranging from 300 to 500 K, NASA TN D-5353, (1969).

[6] F. Kaufmann, R. Möttingdörfer, S. Roth, and M. Schmidt: Investigation of coupling efficiency in laser beam welding of copper materials using brilliant infrared and green laser radiation, J. Manuf. Process. 131, (2024), 2037.

[7] S. T. Auwal, S. Ramesh, F. Yusof, and S. M. Manladan: A review on laser beam welding of copper alloys, Int. J. Adv. Manuf. Technol. 96, (2018), 475.

[8] S. Engler, R. Ramsayer, and R. Poprawe: Process Studies on Laser Welding of Copper with Brilliant Green and Infrared Lasers, Phys. Procedia 12, (2011), 339.
[9] S. Kohl, F. Kaufmann, and M. Schmidt: Why Color Matters—Proposing a Quantitative Stability Criterion for Laser Beam Processing of Metals Based on Their Fundamental Optical Properties, Metals 12, (2022), 1118.
[10] D. Bartels, D. Lang, and J. Schrauder: Laser welding with green and infrared lasers: Influence of the laser wavelength on process characteristics in laser welding of copper, Wiley, (2025), 23.
[11] S. Grabmann, J. Kriegler, F. Harst, F. J. Günter, and M. F. Zaeh: Laser welding of current collector foil stacks in battery production–mechanical properties of joints welded with a green high-power disk laser, Int. J. Adv. Manuf. Technol. 118, (2022), 2571.
[12] S. Grabmann, L. Tomcic, and M. F. Zaeh: Laser beam welding of copper foil stacks using a green high power disk laser, Procedia CIRP 94, (2020), 582.
[13] S. Kamat, W. Cai, T. J. Rinker, J. Bracey, L. Xi, and W. Tan: A novel integrated process-performance model for laser welding of multi-layer battery foils and tabs, J. Mater. Process. Technol. 320, (2023), 118121.
[14] D. B. Hann, J. Iammi, and J. Folkes: A simple methodology for predicting laser-weld properties from material and laser parameters, J. Phys. D: Appl. Phys. 44, (2011), 445401.
[15] J. Ye, S. A. Khairallah, A. M. Rubenchik, M. F. Crumb, G. Guss, J. Belak, and M. J. Matthews: Energy Coupling Mechanisms and Scaling Behavior Associated with Laser Powder Bed Fusion Additive Manufacturing, Adv. Eng. Mater. 21, (2019), 1900185.
[16] M. Döring, M. Gehring, and M. Schmidt: Trans-Conductive Melt Pool Scaling and its Implications for Parameter Transfer in Laser Powder Bed Fusion for Metals with High Thermal Diffusivity, Adv. Eng. Mater. 27, (2025), 2401958.
[17] F. Kaufmann, O. Hentschel, S. Roth, and M. Schmidt: Effects of different laser wavelengths on process performance and weld seam properties in copper processing for electric vehicle applications, Opt. Laser Technol. 191, (2025), 113274.
[18] T. J. Rinker, M. M. Pour, W. Wen, M. E. McGovern, S. Xiang, and W. Cai: Investigating the Welding Limit of Copper Foils to a Tab for Battery Applications with a Green Laser, J. Mater. Eng. Perform. 35, (2026), 355.
[19] V. Mann, F. Hugger, S. Roth, and M. Schmidt: Influence of Temperature and Wavelength on Optical Behavior of Copper Alloys, Appl. Mech. Mater. 655, (2014), 89.
[20] J. R. Davis, Ed. *Copper and copper alloys* (ASM specialty handbook). Materials Park, Ohio: ASM International, (2001).

(Received: June 22, 2026, Accepted: August 23, 2026)